ISSN 1063-7834, Physics of the Solid State, 2019, Vol. 61, No. 12, pp. 2348–2352. © Pleiades Publishing, Ltd., 2019.
Russian Text © The Author(s), 2019, published in Fizika Tverdogo Tela, 2019, Vol. 61, No. 12, pp. 2344–2348.

SEMICONDUCTORS

Studies of Thermoelectric Properties of Superlattices Based on Manganese Silicide and Germanium

M. V. Dorokhin[a,*], Yu. M. Kuznetsov[a], V. P. Lesnikov[a], A. V. Zdoroveyshchev[a], P. B. Demina[a], and I. V. Erofeeva[a]

[a] *Research Institute of Physics and Technology, Lobachevsky State University of Nizhny Novgorod, Nizhny Novgorod, 603022 Russia*

**e-mail: dorokhin@nifti.unn.ru*

Received July 16, 2019; revised July 16, 2019; accepted July 25, 2019

Abstract—In this paper, we present the results of the study of thermoelectric materials formed by pulsed laser deposition on sapphire substrates and representing thin $MnSi_{1.74}$ films with intermediate germanium layers. A sharp decrease in the thermal conductivity coefficient of superlattices based on manganese silicides and germanium in comparison with single layers of manganese silicide with an equivalent thickness is shown. This allows significantly increasing the thermoelectric figure of merit. The obtained values of the coefficient of thermoelectric figure of merit are comparable with the known literature values that are typical for similar structures.

Keywords: thin films, higher manganese silicide, superlattices, Seebeck thermoelectric effect, thermoelectric figure of merit

DOI: 10.1134/S1063783419120102

1. INTRODUCTION

In view of environmental issues associated with operation of modern technological methods for generating electric energy, alternative energy sources, the principle of which does not harm the environment, are actively being developed. Solar panels, betavoltaics, hydrogen cells, and hydrogen fuel are a small list of directions for the development of an environmentally friendly method for generating electric energy [1]. One of promising research areas is the development of thermoelectric energy converters. Thermoelectrics are the materials producing electrical voltage when creating a temperature gradient on opposite faces.

The main parameter characterizing the performance of the future thermoelectric energy converter is the dimensionless thermoelectric figure of merit $ZT = \alpha^2 T/\sigma\lambda$, where λ is the thermal conductivity coefficient, σ is the electrical conductivity, α is the Seebeck coefficient, and T is the average temperature of the structure.

To achieve high parameters of thermoelectric quality factor ($ZT \approx 1$–3), it is necessary to develop a material with a high electrical conductivity and low coefficient of thermal conductivity. The optimal ratio of parameters is achieved in heavily doped semiconductors. However, a limited number of publications, in which getting ZT greater than unity is reported, are known for bulk semiconductor materials [2, 3]. Since the ZT coefficient is directly related to the efficiency, the low characteristic ZT values do not allow, in most cases, to obtain a material competitive in comparison with other methods of generating electric energy. Moreover, thermal and electrical parameters included in the formula for ZT depend on each other within the same material: with an increase in electrical conductivity, an increase in the thermal conductivity is observed due to an increase in the contribution to heat transfer by free charge carriers and a Seebeck coefficient decreases due to a change in the Fermi level position (deeper into the conduction or valence bands, depending on the type of material conductivity).

A significant segment of modern research on the subject [4–9] is aimed at the development of thermoelectrics based on chemical compounds with a complex crystal structure consisting of two types of significantly different atom sizes (for example, higher manganese silicide). By applying this approach, it is possible to achieve a mismatch of phonon spectra in order to reduce the phonon component of the thermal conductivity coefficient [4]. Creation of superlattices containing such materials and intermediate layers provides additional phonon scattering at heteroboundaries. This approach allows reducing the thermal conductivity coefficient even more significantly [10, 11].

This paper is aimed at studying the thermoelectric properties of nanoscale films, which are single and multilayer structures consisting of a manganese silicide compound in composition close to higher man-

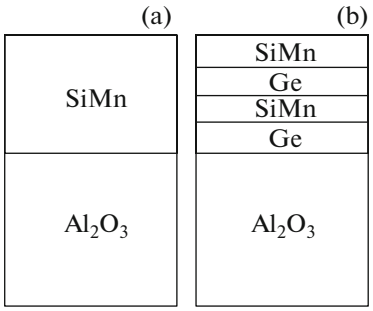

Fig. 1. Schematic diagram of the studied structures: (a) single HMS layer, (b) superlattice of HMS and Ge layers.

ganese silicide (HMS) $MnSi_{1.74}$ (Fig. 1a) and intermediate germanium layers (Fig. 1b).

2. METHODOLOGY OF THE STRUCTURE FORMATION

The films were formed by pulsed laser deposition (PLD) in vacuum. The targets were a *p*-type germanium plate and a higher manganese silicide target sintered from nanopowders by spark plasma sintering (SPSM 15) [12]. The use of presintered material with a desired composition as a target allows obtaining films with a determined manganese concentration.

Targets were sputtered by pulsed Nd : YAG lasers operating in the Q-switched mode. The sputtered material was deposited on a sapphire substrate, the temperature of which was 350°C. At depositing a uniform $MnSi_{1.74}$ film, a target of higher manganese silicide was continuously sputtered during the entire deposition process (~40 min). Upon deposition of the $MnSi_{1.74}$/Ge multilayer structure, alternate sputtering of targets of higher manganese silicide and *p*-Ge was carried out. The thickness of each layer was set by a change in the time of sputtering of targets. Table 1 shows a list of structures with the indication of technological formation parameters of each layer. Structures differ in relative thicknesses of layers.

All structures have the same total thickness of a deposited film (as estimated by sputtering time), but differ in the absolute thickness of the layers in it and the number of periods. Structure 1 is relatively homogeneous $MnSi_{1.74}$ layer, and this structure was formed to compare the results.

After growth, ohmic gold-containing contacts were formed on the surface of the studied structures by electron beam evaporation in vacuum for the subsequent study of the Seebeck coefficient. The formed contacts had thermal stability in the studied temperature range (50–450°C).

3. EXPERIMENTAL METHODOLOGY

When measuring the Seebeck coefficient, the sample edges were placed on two independent heaters, the temperature of which was set and maintained by PID temperature controllers. During the experiment, a constant difference of the temperatures of around 10 K was maintained between the sample edges. The sample was pressed to the heaters with two molybdenum clamps (see Fig. 2) for better thermal contact between the sample and the heater. Due to its low coefficient of thermal expansion, molybdenum is used to prevent mechanical damage to the structure when the metal is heated. Flat thermocouples were placed between the sample and the clamps while their output contacts were attached to a thermostated area in a vacuum chamber. Voltages of thermocouples were recorded using the L-Card E-140 data acquisition system. Thermocouple readings are proportional to the temperatures of the upper face of the studied structure. Voltage measured with the same type of contact ("chromel–chromel" U_{Ch}, "alumel–alumel" U_{Al}) are proportional to the emerging thermo-EMF with allowance for the thermoelectric effect of the chromel α_{Ch} and alumel α_{Al}. The Seebeck coefficient of the structure: $\alpha_s = \alpha_{Ch} + U_{Al}(\alpha_{Ch} - \alpha_{Al})/(U_{Al} - U_{Ch})$.

The main advantage of the above methodology is the absence of the need to measure the true value of the temperature difference since the Seebeck coefficient of the structure is determined by comparing the

Table 1. Parameters of samples obtained by spark sintering

Structure no.	Targets	Structure composition	Target sputtering time, min	Structure thickness, nm
Struct 1	1—PSM-15	$MnSi_{1.7}$	PSM 15—73′	50
Struct 2	1—PSM 15	$[MnSi_{1.7}/Ge]_6$	SPSM 15—6′	50
	2—Ge		Ge—6′	
Struct 3	1—SPSM 15	$[MnSi_{1.7}/Ge]_6$	SPSM 15—9′	50
	2—Ge		Ge—3′	
Struct 4	1—SPSM 15	$[MnSi_{1.7}/Ge]_{12}$	SPSM 15—3′	50
	2—Ge		Ge—3′	

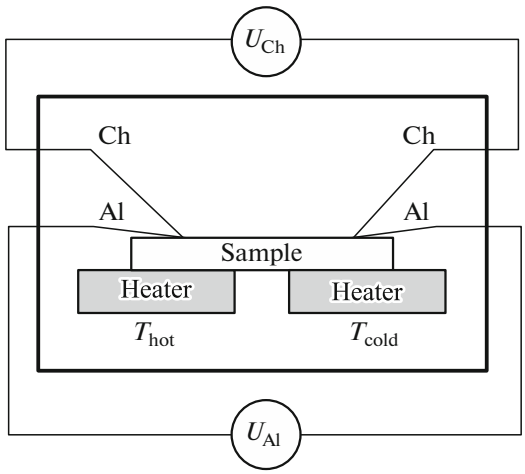

Fig. 2. Schematic diagram of the Seebeck coefficient measurement: Al—alumel; Ch—chromel; Heater—ovens; Sample—test sample; U_{Al}, U_{Ch}—voltmeter that records the thermo-EMF from the alumel and chromel branches, respectively; T_{hot}, T_{cold}— temperatures of "hot" and "cold" ovens, respectively.

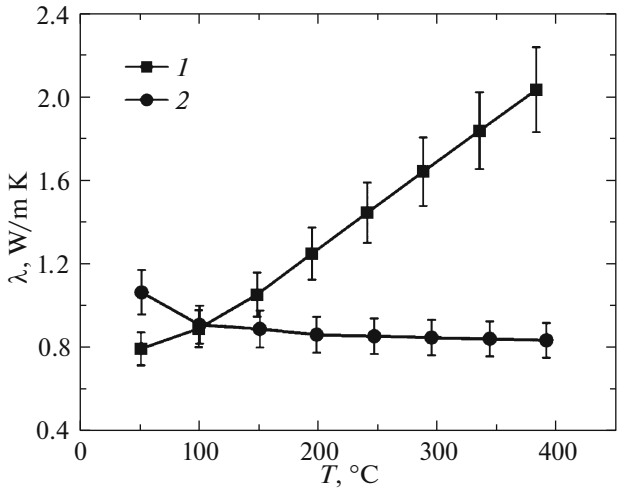

Fig. 3. Experimentally obtained temperature dependence of the thermal conductivity coefficient: (*1*) single HMS layer, (*2*) HMR- and Ge-based superlattices.

emerging thermo-EMF relative to chromel and alumel. The average temperature was calculated by the formula: $T = (T_{hot} + T_{cold})/2$, where T_{hot} and T_{cold} are temperatures of the first and second heaters, respectively (see Fig. 2).

The resistivity of the sample was measured using a standard four-probe method.

The value of the thermal conductivity was measured by the method of frequency separation (3ω-method) [13, 14]. During measurements of the resistance and thermal conductivity coefficient, a zero temperature difference between the faces of the sample was ensured.

All measurements were carried out in vacuum at residual vapor pressure of 10^{-3} Torr to reduce heat removal by air from heated areas of the sample and reducing sample degradation due to atmospheric exposure.

As a result of the studies, the temperature dependences of the Seebeck coefficient, resistivity, thermal conductivity coefficient, and thermoelectric figure of merit of formed structures were analyzed.

4. EXPERIMENTAL RESULTS

Based on the obtained temperature dependences of the thermal conductivity coefficient of the structures (Fig. 3), the value of λ for a single HMS layer is comparable with published data [2]. In this case, we note that the thermal conductivity coefficient at a temperature below 100°C is higher for a multilayer structure than for a single HMS layer and is lower for a multilayer structure than for a single HMS layer at $T >$ 100°C. A decrease in the thermal conductivity coefficient in a multilayer structure is due to additional phonon scattering at the boundary of the $MnSi_{1.74}$ and Ge layers. At temperatures below 100°C, the scattering effect at the boundaries is leveled due to a higher value of the thermal conductivity coefficient of Ge [15–17] (as a result, the λ value averaged over the film thickness, which is calculated using the 3ω method, becomes higher). However, at increasing temperature, the value of thermal conductivity coefficient of Ge is significantly reduced, and this leads to a decrease in the total λ value.

The temperature dependences of the electrical resistivity (Fig. 4) show that close ρ values are specific to all structures, with the exception of structure 4.

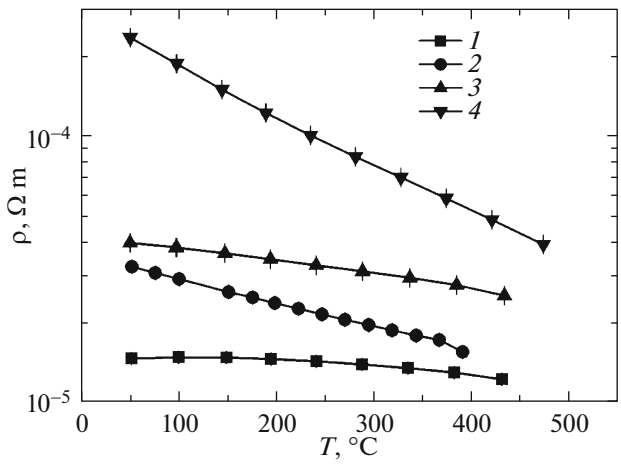

Fig. 4. Experimentally obtained temperature dependence of the resistivity coefficient of the studied structures: (*1*) structure 1, (*2*) structure 2, and (*3*, *4*) structures 3 and 4, respectively.

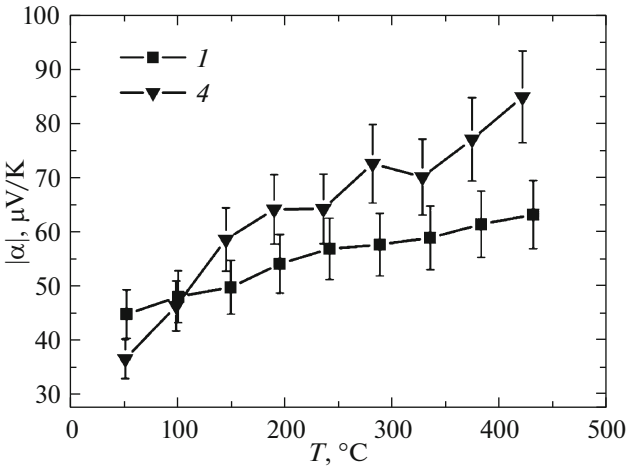

Fig. 5. Experimentally obtained temperature dependence of the Seebeck coefficient of the studied structures: (*1*) structure 1, (*4*) structure 4.

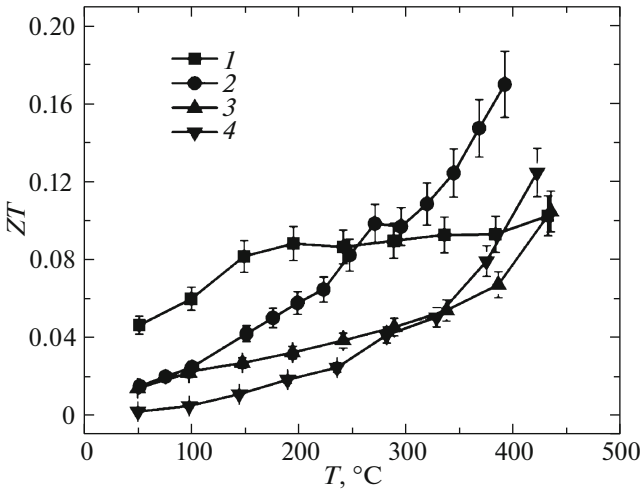

Fig. 6. Temperature dependence of the thermoelectric figure of merit of the studied structures calculated based on the obtained experimental data: (*1*) structure 1, (*2*) structure 2, and (*3*, *4*) structures 3 and 4, respectively.

Structure 1 (curve *1*), which is thick single HMS layer, has the lowest resistance. The presence of an intermediate Ge layer leads to an increase in resistance of all thicknesses considered. The increase in resistance in multilayer structures can be explained mutual diffusion of Ge and Mn atoms. Mutual diffusion presumably leads to the formation of additional (for example, GeMn) phases in the film, which is accompanied by the appearance of internal potential barriers that prevent both the current flow between layers and the increase in electrical resistance of the applied film. The indicated effect is most pronounced for a multilayer structure with the smallest period (structure 4—curve *4*). In the case of a small thickness of each individual layer, potential barriers arising from the appearance of new phases most effectively block the current transfer through this layer.

Since the temperature dependences of the Seebeck coefficient for structures 1–3 (Fig. 5) coincide within the error range, the graph shows the curves of structures 1 and 4. Analyzing the temperature dependence of the Seebeck coefficient, we can conclude that the magnitude of the effect correlates with the magnitude of the resistivity. Thus, structure 4 with the highest resistance has the highest thermo-EMF value. However, the thermoelectric efficiency of this layer is the worst of the presented superlattices. The highest *ZT* value (Fig. 6) was obtained for structure 2 and is 0.18, which is comparable with the values obtained early [3, 13, 14, 18, 19].

Obviously, an increase in the film heterogeneity due to the introduction of germanium layers has a negative effect on the current transfer for all studied structures. The increase in resistance is accompanied by a decrease in *ZT* values. At the same time, the negative effect of Ge on electrical properties is totally compensated by a decrease in the thermal conductivity in multilayer structures. At optimal selection of the layer thickness, this allows increasing the coefficient of the thermoelectric figure of merit compared to that for homogeneous layer of higher manganese silicide.

5. CONCLUSIONS

In this paper, we studied the thermoelectric properties of thin HMS films formed on the sapphire substrate by the PLD method, as well as of superlattices consisting of HMS layers and intermediate germanium layers. The introduction of intermediate low-resistance layers is experimentally confirmed to allow creating an additional object of heat dissipation in the structure, i.e., the interface between layers, which promotes to reduce the thermal conductivity coefficient at maintaining the magnitude of the Seebeck effect.

It is important to note that we show here an additional technological degree of freedom for control of thermoelectric parameters of the superlattice by the variation of the main and intermediate layers. This allows completely compensating for the negative effect of increasing the resistance at the introduction of Ge layers and slightly increasing the *ZT* coefficient.

ACKNOWLEDGMENTS

The authors thank A.V. Boryakov for SEM studying the target composition and M.S. Boldin for target sintering experiments.

FUNDING

This work was supported by the Russian Science Foundation, project no. 17-79-20173.

CONFLICT OF INTEREST

The authors declare that they have no conflicts of interest.

REFERENCES

1. J. Mahtashan, Energy Proc. **74** (2015).
2. C. Gayner and K. K. Kar, Prog. Mater. Sci. **83**, 330 (2016).
3. Z.-G. Chen, G. Han, L. Yang, L. Cheng, and J. Zou, Mater. Int. Progr. Natur. Sci. **22**, 535 (2012).
4. L. Ivanova, J. Thermoelectricity **3**, 60 (2009).
5. S. Saini, P. Mele, H. Honda, K. Matsumoto, K. Miyazaki, and A. Ichinose,J. Electron. Mater. **43**, 2145 (2014).
6. M. V. Dorokhin, I. V. Erofeeva, Yu. M. Kuznetsov, M. S. Boldin, A. V. Boryakov, A. A. Popov, E. A. Lantsev, N. V. Sakharov, P. B. Demina, A. V. Zdoroveyshchev, and V. N. Trushin, Nanosyst.: Phys. Chem. Math. **9**, 622 (2018).
7. S. Bathula, M. Jayasimhadri, N. Singh, A. K. Srivastava, J. Pulikkotil, A. Dhar, and R. C. Budhani, Appl. Phys. Lett. **101**, 213902 (2012).
8. E. Witkoske, X. Wang, M. Lundstrom, V. Askarpour, and J. Maassen, J. Appl. Phys. **122**, 175102 (2017).
9. I. A. Tombasov, Fiz. Tverd. Tela **60**, 12 (2018).
10. Y. Chandel, Int. J. Sci. Res. **4**, 6 (2015).
11. A. Kandemir, A. Ozden, T. Cagin, and C. Sevik, Sci. Technol. Adv. Mater. **18**, 187 (2017).
12. M. V. Dorokhin, I. V. Erofeeva, Yu. M. Kuznetsov, M. S. Boldin, V. P. Lesnikov, A. V. Boryakov, A. A. Popov, E. A. Lantsev, N. V. Sakharov, P. B. Demina, A. V. Zdoroveyshchev, and V. N. Trushin, Nanosyst.: Phys. Chem. Math. **9**, 622 (2018).
13. K. T. Wojciechowski, R. Zybala, and R. Mania, J. Achievem. Mater. Manuf. Eng. **37**, 2 (2009).
14. D. Cahill, Rev. Sci. Instrum. **61**, 802 (1990).
15. F. Schaffler, E. Levinshtein, S. Rumyantsev, and M. Shur, *Properties of Advanced Semiconductor Materials: GaN, AIN, InN, BN, SiC, SiGe* (Wiley, New York, 2001).
16. F. Schäffler, Semicond. Sci. Technol. **12**, 1515 (1997).
17. H. Stöhr and W. Klemm, Z. Anorg. Allgem. Chem. **241**, 305 (1939).
18. X. Chen, A. Weathers, A. Moore, J. Zhou, and L. Shi, J. Electron. Mater. **41**, 6 (2012).
19. S. Joo, H. Lee, J. Lee, and J. Jang, J. Alloys Compd. **747**, 1 (2018).

Translated by A. Ivanov